LIST OF ILLUSTRATIONS

ACKNOWLEDGEMENTS

We wish to acknowledge the various United States Coast Guard groups which made the entire field test effort possible. Among these are the Electronics Center at Wildwood, N.J., who loaned the vehicle; the flight crews from Elizabeth City, N.C. who flew the van to and from California; LT. JG W. F. Nettle and his people in Manned Units Liaison at Yerba Buena who moved our equipment to the lighthouse at Pt. Bonita and then carried it back for us; and the men of the Light, particularly Ch. H. Hoffman and J. Emrick, for their help and patience during our stay with them.

INTRODUCTION

During the month of September, 1971, the authors, members of the Optical Devices Group of the Radar and Navigation Branch at TSC, performed field tests at the Coast Guard Lighthouse, Point Bonita, California. The tests, which were carried out in cooperation with the Coast Guard under PPA, CG-202, were intended to determine several unknown factors which are decisive in the selection and final design of a prototype Fog Bank Detector. In particular, two systems were under test: a ruby laser LIDAR (for detecting fog banks by optical backscattering) and an infrared radiometer (whose detection principle is based on the emittance differences of water, sky and fog at wavelengths in 8 to 13 μ atmospheric window)[1].

The purpose of these tests was to assess the performance of the two candidate systems under actual fog bank conditions. The type of fog bank of particular interest to the Coast Guard is generally prevalent on the West Coast during certain times of the year. It has been expected, on the basis of previous local experience at Point Bonita, that fog bank occurrence would be frequent during September, allowing the efficient use of test time. Unfortunately, the weather was unseasonably warm during most of the tests, and, though there was some fog, it was primarily due to the lowering of ceiling on overcast days. Since the variety of fog desired for the tests was a moving bank approaching across the water on a clear day, the test conditions were far from ideal.

However, several important conclusions were drawn from observations, both qualitative and quantitative, made during the 28 day period. For example, considerable data were obtained on LIDAR backscattering from clouds, including banks formed by the breaking up of fog. From these data, measures of reflected pulse widths, peak return powers and reflectance variability within the same cloud could be found. In addition, the background

seen by the receiver due to sunlight scattered from the (target) clouds was determined. The infrared technique was found to produce ambiguous results under the variety of sky cover conditions, including haze, which were met.

The specific tasks which were to be carried out in these tests are outlined below:

1. Equipment Checkout (Alignment, Calibration, etc.)
    - LIDAR
        - Alignment of laser (ruby);
        - Q-switching of laser;
        - Calibration of laser (pulse energy, width, beam divergence);
        - Alignment of LIDAR;
            - Adjust field of view;
            - Align axes of transmitter and receiver (coaxial);
            - Measure range of known targets.
    - Infrared Radiometer
        - Mount radiometer at appropriate location and height above sea-level (at least 20 meters);
        - Measure drift of zero level and reduce to acceptable level by suitable baffling and insulation;
        - Align viewing scope with radiometer.
        - Observe radiance difference between sky and sea on clear day and night.
        - Establish a reference object for scanning (e.g., a permanent structure on the beach or an artificial target).
    - Videograph
        - Install Videograph B (on loan to TSC from the USCG).
        - Check calibration of detector.

2. Field Experiments

- LIDAR
  - Measure peak intensity of return pulses from fog bank;
  - Observe the variation in the return intensity, if any, from the same fog bank, due to possible patches or structure in the fog.
  - Measure broadening of pulses reflected from fog banks.
  - Measure background radiance, especially from sun-lit clouds.
  - Measure strength of atmospheric backscatter, as a function of visibility.
  - Observe physical characteristics of fog banks, including widths, heights and motion.
  - Test bistatic configuration, especially with regard to the GaAs LIDAR design.
- Infrared Radiometer
  - Measure the effective temperature difference between the sea surface and the fog bank, as well as the variance in this temperature difference.
  - Determine the softness of the fog bank; i.e., how well is it defined? Is the shape of the infrared signal usable in detection or is it too ambiguous?
  - Determine the effect of potential sources of interference (e.g., ship exhausts, sea surface changes due to wind, wakes, etc.)
  - Is scanning in a single vertical plane sufficient, or must horizontal scan be provided?

All the above tasks were completed, with the exception of those which refer specifically to fog banks. (For example, we

could not determine the softness, or the height or extent of typical banks, due to their limited occurrence as described previously.) Furthermore, the bistatic LIDAR configuration was not tried. The bistatic alignment is difficult to perform in the field, and there was apprehension, especially as the test period drew toward the end, that the system might not be returned to proper alignment in time if the appearance of a fog bank were imminent.

The remainder of the report discusses the conditions under which the field tests were carried out, the physical and geographical features of the test site, and the apparatus used. The procedures for data taking are presented for each of the two candidate methods. The data analysis is then summarized and the conclusions stated with regard to selection of a fog bank detector.

FIELD TEST SITE

Equipment needed for the field tests was prepared at TSC and loaded on a medical coach van on loan from the U.S. Coast Guard Electronics Command, Wildwood, New Jersey. The van, though outfitted for field use as received (with a 20 KW gasoline operated generator), was used by us for transportation only. Thus the loaded vehicle was driven to Hanscom Field, Bedford, Mass., where it was driven onto a Coast Guard C-130 Aircraft and flown to the San Francisco Coast Guard Air Station. The authors met the van and drove it to Point Bonita Light Station, which is situated on the south-western tip of Marin County, just across the Golden Gate from San Francisco. Fig. 1 shows a map of the area, and is adapted from a portion of Coast and Geodetic Survey chart #5532.

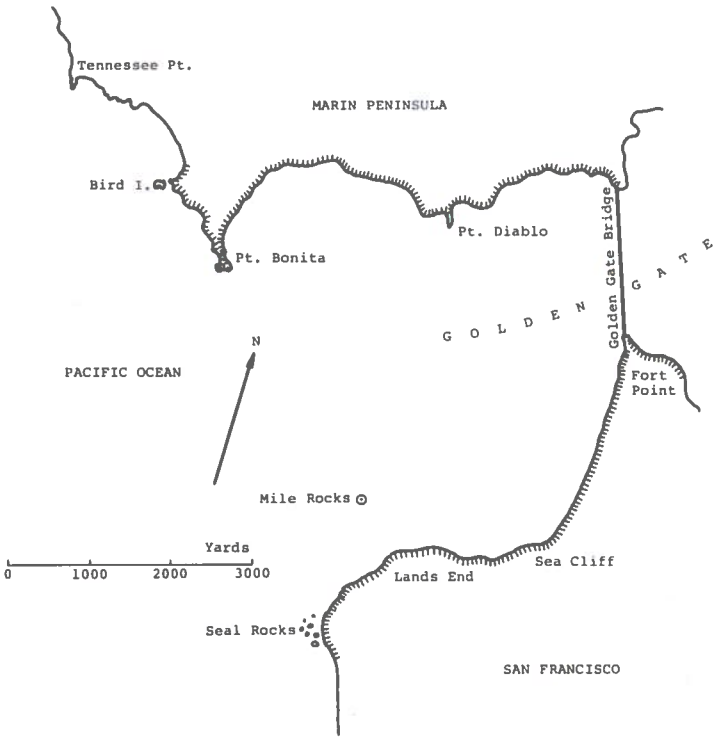

Figure 1. Map of Golden Gate Area Showing Point Bonita and Other Locations Relevant to Field Tests (Adapted from C+GS Chart #5532).

The experiments were to be conducted from the lighthouse, or more specifically from the generator house attached to the lighthouse. This meant that the equipment, including several pieces weighing over 300 lbs, had to be transported over a rugged path approximately 3/4 mile long and less than five feet wide in places. In addition, the path wound up and down the side of a cliff and passed through a 75-foot tunnel approximately 6 1/2 feet high and 5 feet wide. The moving task was accomplished with the help of personnel from the Coast Guard District Headquarters on Yerba Buena. A four-wheel drive jeep-like vehicle, dubbed the "Mule", was used and was perfect for this particular job.

The generator house had windows on all sides (see Figure 2). It was adequately spacious to allow the setting up of the instruments and apparatus, storage of empty crates, and construction of temporary office and eating space. A narrow walk, protected by a railing, surrounded the structure on all sides and offered unobstructed views to the north, west and south. Beyond the railing was a precipitous drop of about 100 feet to the rocks and waves below.

Referring to Figure 2, the northern window overlooks Bird Island and other promontories along the coast; the westerly windows overlook the open sea and from the windows to the south, one sees the northwestern part of San Francisco. From the position on the outer walk, marked A in Figure 2, it is possible to see a region encompassing more than 180°, reaching from the Golden Gate Bridge, to the east, to the open sea in the west. Because of the desirability of this particular aspect, the LIDAR was installed outside in position A. Support cables and tubing for power and cooling were brought through a nearby window from the power supply and temperature controller located inside the generator house. Since the LIDAR was mounted on a wheelable tripod, the actual horizontal field covered was close to 210°. Because of the generally mild weather, it was found that the

LIDAR could be safely left outside around the clock, covered at night only with a plastic tarp to protect it from salty spray.

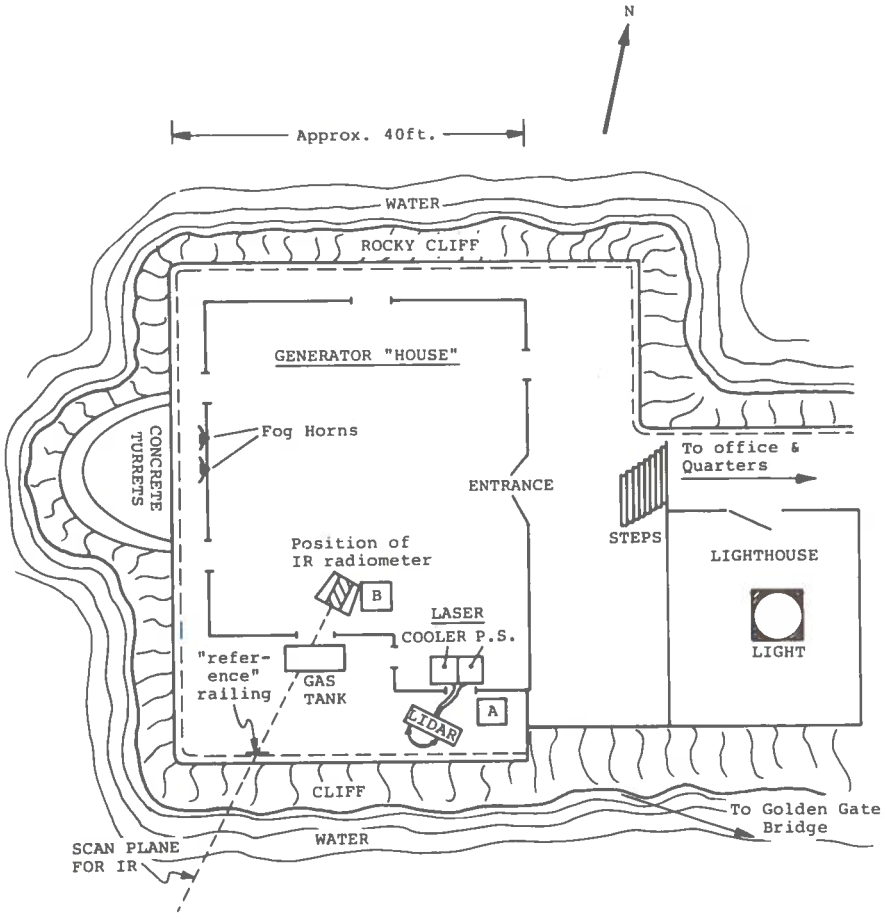

Figure 2. Plan of Point Bonita Lighthouse Area Showing Location of Installation of LIDAR (A) and IR Radiometer (B). (Scale is only approximate)

The infrared radiometer was initially installed in the western window, just north of the fog horn. However, the wind was generally quite strong from the west and northwest and this made the radiometer too unstable to use; therefore it was moved to the position B, shown in Figure 2. This allowed the radiometer to scan in a vertical plane (which intersects the plane of the figure in a line running approximately north/south, and which could be slightly altered so as to either include or exclude a stretch of land in the scan).

LIDAR EXPERIMENTS

DESCRIPTION OF APPARATUS

The LIDAR has been described in some detail in Appendix B of Reference 1. The ruby laser (λ=6943Å) contained a 3" x 1/4" rod and was Q-switched with a pthalocyanine-in-nitrobenzene dye solution. A p-i-n diode was placed behind the 99% reflector to serve as a monitor of the laser pulse, and also provide a trigger pulse to the oscilloscope when needed.

The laser was aligned at the outset of our tests without the Q-switch dye. The dye cell was then added and by trial-and-error the desirable level of Q-switching, with single, narrow pulses, was obtained. Once aligned in this fashion, the laser remained in alginment for the entire duration of the tests, and the output pulses were never observed to deviate by more than 50% in peak power during this time. In general, except near the end of the test period, when the weather began to take its toll on some of the components, the variation in peak power was no more than $\pm$ 10%.

The peak power of the output pulse was determined by measuring the pulse energy with a Quantronix energy meter and the pulse width as displayed on an oscilloscope. The measured energy of 220 mJ ($\pm$10%) and width Δt_0 (30 nsec $\pm$ 10 nsec) leads to a peak pulse power of 7 $\pm$2 Mw.

The LIDAR was used in the coaxial or monostatic mode; i.e., the laser beam was directed through a pair of total reflecting prisms in such a way that it emerged along the optical axis of the receiver system. (See Figure B1 of Reference 1.) By means of the exit prism (the prism on the receiver optical axis), the direction of the laser beam could then be altered as necessary, for the LIDAR alignment.

The receiver optical system is shown schematically in Figure 3. Light from the target fog bank or cloud is incident

on the 25 inch focal length, f/5 receiver objective and passes through an adjustable aperture which limits the field-of-view (f.o.v.) Lens L_1 serves to collimate the beam before it passes through the optical filters. Lens L_2 distributes the light over a large fraction of the area of the photocathode. The diameter of the beam passing through the narrow-band and neutral density filters was 3/4 inch. This was also the approximate size of the illuminated spot on the photocathode.

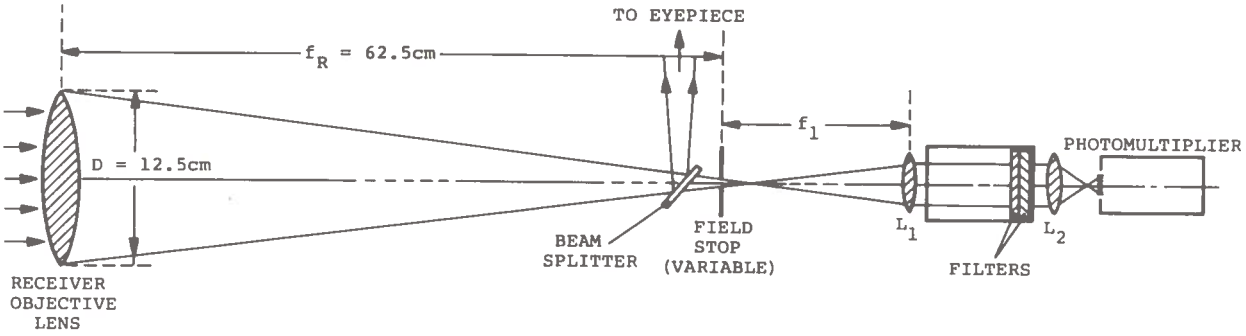

Figure 3. LIDAR Receiver Optics

The photomultiplier used was an EMI 9558B tube with S-20 response.

ALIGNMENT OF THE LIDAR

The LIDAR must be aligned so that the receiver looks at the same region of space illuminated by the laser beam. Since the system was used in the coaxial mode, this alignment consists of assuring that the laser beam emerges from the second totally reflecting prism at a point along the optical axis of the receiver and making the direction of the laser beam parallel with that same axis. The divergence of the laser beam was two to three mrad. For a restricted receiver f.o.v. (determined by the field aperture setting) misalignment will result in loss

of signal reflected from a target.

Alignment was carried out as follows. First the prism P_2 (see Figure 4) was positioned as close to the optical center of the objective lens as it was possible to determine by eye. The laser was then fired and the position of the spot on a near target (cardboard or rock surface) noted in the monitoring eyepiece. This eyepiece has been aligned previously to look (via a 45° beam splitter) along the optical axis of the receiver. The prism P_2 was then adjusted in angle (but not position) until the laser spot appeared in the center of the field-of-view

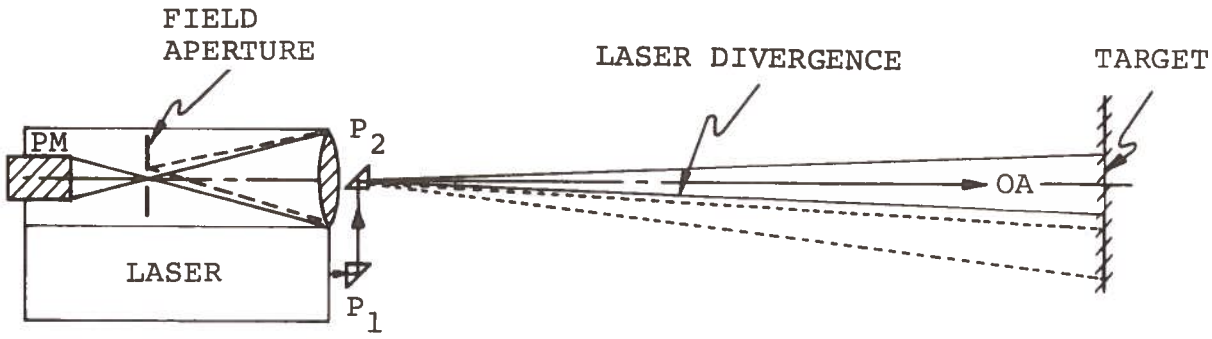

Figure 4. Diagram Showing Role of Prism P_2 in Determining Alignment of Laser Beam with Respect to Receiver Field-of-View. Dotted Beams Represent the Misalignment Laser and its Return Signal. The Field-of-View of the Receiver is Assumed to Equal the Laser Divergence Angle, for this Example.

of the eyepiece. By using two targets at distances of 30 feet and 500 feet, respectively, the alignment was made successively finer. Figure 5 shows the importance of proper alignment. The target was a vertical cliff somewhere between Lands End and Sea Cliff (see Figure 1) at a distance of approximately 2.5 miles. The aperturing of the misaligned receiver from 10 mm to 3 mm reduced the signal considerably. After alignment, the aperture could be reduced to approximately 1 mm with no significant loss in signal.

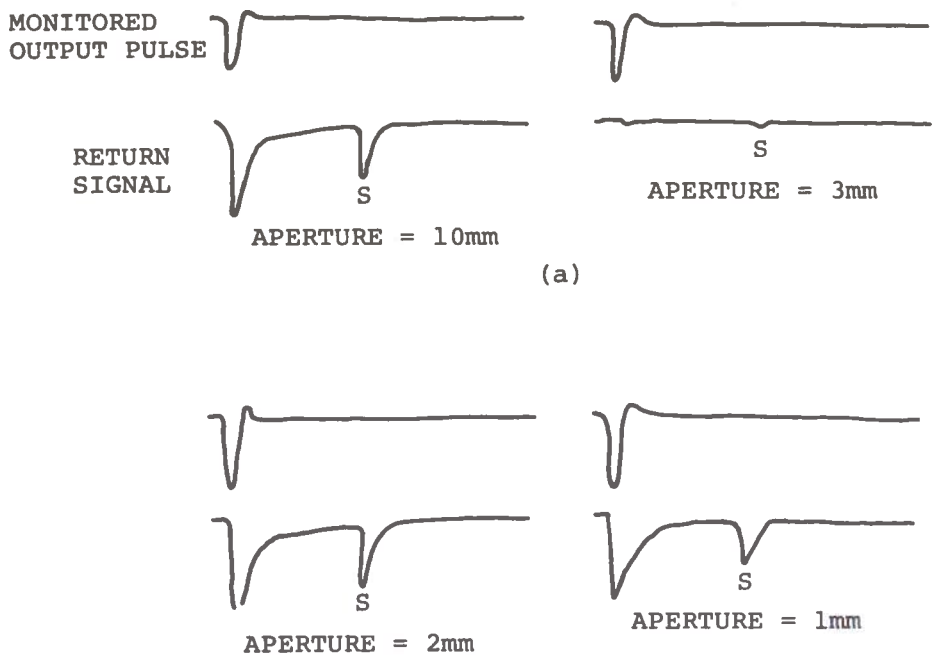

Figure 5. Oscillogram Traces of Laser Output Pulses and Return Signals from a Cliff at 2.5 Miles, Showing Effect of Reducing Field Apertures for (a) Misaligned LIDAR and (b) Aligned LIDAR. The Scales are the Same for All Four Pairs of Traces. "S" Indicates Position of Return Signal

METHOD OF OBSERVATION AND DATA TAKING

The procedure for obtaining data consisted of aiming the LIDAR at a target (low cloud or fog) and firing the laser. The return signal striking the photocathode after passing through the optical filters (Figure 3), caused a current to appear at the output of the photomultiplier. This current passed through an external load resistor R_L and the signal voltage was monitored by a Tektronix 556 dual beam oscilloscope. The scope was generally used in the delayed sweep mode as follows: The A or top trace, triggered by the initial return from the atmosphere, was swept relatively slowly (5 μsec cm^{-1}) and allowed signals arising anywhere from zero feet out to about five miles to be observed. If and only if a signal exceeding a present level was received, the B or bottom trace was triggered and,

on a much faster sweep (e.g., 100 nsec cm^{-1}) this signal was displayed. (See, for example, the signal from the cliffs to the south, Figure 6.) The 556 oscilloscope allows a variable delay to be set so that the B channel will not trigger on any part of the atmospheric backscatter signal.

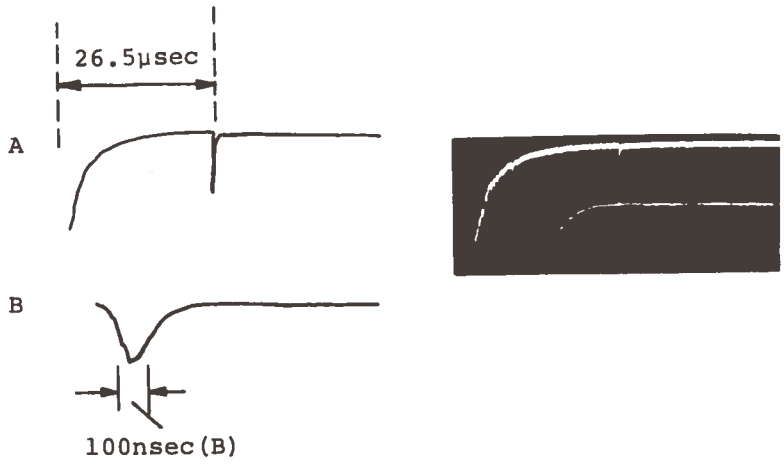

Figure 6. Oscilloscope Trace Showing Use of Delayed Trigger on B (bottom) Trace to Expand Return Pulse. Sweep Settings: A = 5 μsec/cm: B = 100 nsec/cm. Target was a Cliff 2.7 Miles Away

The target and its conditions of sky illumination were photographed in color with a Polaroid "scene" camera and in each case, the photograph was marked at the aiming point of the LIDAR.

The cliffs opposite the lighthouse, from which the signal in Figure 6 was obtained, were used as a source of "ground truth". Periodically, in the course of data collection, the LIDAR was aimed at these cliffs and the resulting traces examined for changes. The results generally confirmed the reproducibility of the LIDAR equipment, with any deviations accountable for in terms of variation in atmospheric transmission (i.e., visibility) or output pulse variations.

The voltage applied to the photomultiplier was varied at first to arrive at a value which was consistent with the maximum desirable current through the tube. By the appropriate selection of narrow band and neutral density optical filters,

the background currents (from the sky or sun-reflections from clouds) were kept generally below 30 μA. Similarly, the peak signal current was maintained below 1 mA in most cases. Detector saturation effects were studied using the signal from the cliffs, and the combination of filters and photomultiplier voltage was chosen to minimize saturation and to allow some dynamic range for signal size (by removing neutral density). In addition, time constant effects due to R_L were studied and R_L selected so that 80 to 100 nsec wide return pulses would not be artificially broadened. The value finally used was R_L = 50 ohms.

One of the objectives of this study was to determine levels of background illuminance from clouds. Fluctuations in this illuminance level were the primary cause of noise in the data presented below. Measurements of the absolute background level therefore served two purposes:

1. To aid in the design of the prototype fog bank detector;
2. To calibrate the internal consistency of the data analysis, since the S/N ratio observed on the oscilloscope is a function of, among other things, the background level.

The measurement of background level requires a knowledge of the spectral characteristics of the narrow band filter. Early data was taken with a 10Å filter which, being so narrow, is inherently sensitive to angle and to ambient temperature. Since the shifting of the peak wavelength of such a filter could cause a serious and unknown change in its transmission at the laser wavelength, it was replaced by a 100Å filter. At the same time, a spurious light leak was discovered in the filter chamber, which only manifested itself when the sun was in a particular part of the sky. For these reasons, the early data were not included in the analysis. In retrospect, there appears to be no problem with the 10Å filter (that is, the early data

are consistent with the later data); however, the light leak did cause excessive background levels to be measured.

Finally, an important quantity which comes into the analysis of the LIDAR data is the visibility. Since the visibility ($\simeq 4/\gamma$, where γ is the atmospheric extinction coefficient) enters the expression for return power in the exponent (see Equation 3-6 of Reference 1), quantitative use of backscatter data will depend on accurate knowledge of visibility. This was a serious problem in the field test situation. The visibility was often inhomogeneous over the Bay. An Impulsephysik Videograph Fog Detector had been brought with the rest of the equipment, but was not giving accurate readings. It was felt however, that the Videograph, even if properly calibrated, would not provide a useful measurement of the visibility (because of the variation of visibility conditions with elevation and direction). Instead, targets were chosen at various distances and the visibility was estimated by eye. This method proved to have weaknesses, too, and the errors resulting caused some values deduced from the experiments (in particular, the cloud reflectivities) to be unrealistic.

CALIBRATION OF APPARATUS

In order to make quantitative use of the backscatter data, various system measurements and calibrations are required. These are as follows:

1. Field-of-View of the Receiver - The field-of-view was determined by removing the photodetector and examining a given scene in the field lens (L_2) following the filter box (Figure 3). The scene used was the Golden Gate bridge at a distance of 15,000 feet (determined from a scale map). The field aperture was closed until two successive suspension cables framed the field-of-view. The separation between cables is 50 feet and the aperture diameter needed was 1.5 mm.

Therefore, the (full angle) f.o.v. = 50/15,000 = 3.3 mrad at 1.5 mm aperture or 2.2 mrad/mm of aperture.

2. Effective Areas of Receiver -

Lens diameter = 12.5 cm

" area = 117 cm^2

Area obscured by prism = 4 cm^2

Effective area = 113 cm^2 = A_R

3. Photomultiplier Calibration - On return to the Boston area, the photomultiplier was sent to the Metrology Laboratory of EG&G, Inc., Bedford, Mass., for calibration. The values found for the responsivity of the phototube at 6943Å were 2.03×10^4 A $watt^{-1}$ (@ 1000 volts) and 1.48×10^5 A $watt^{-1}$ (@ 1250 volts). The responsivity measurements were made at 75 °F. A 3/4 inch aperture was placed 1 3/8 inch in front of the photocathode during this calibration to duplicate the area used in the field experiments. The dark current at 1000^V was found to be 7.3×10^{-10}A.

4. Calibration of Optical Filters - Filters were measured on a Hitachi Recording Spectrophotometer. The results:

Neutral density = 1: Transmission at 6943Å = 0.075

Neutral density = 2: Transmission at 6943Å = 0.015

Narrow Band at 6943Å:

$\Delta\lambda$ = 10Å; Transmission = 0.15

$\Delta\lambda$ = 100Å; " = 0.77

The overall transmission of the receiver optical system (exclusive of filters) has been estimated, for the purpose of carrying out the analysis, to be 0.3.

ANALYSIS OF LIDAR DATA

Uses of the Data

The analysis of the LIDAR data has been done with respect to several relationships developed in Reference 1.

Backscatter Signal

The magnitude of the signal power P_R' reflected from fog or cloud, and reaching the photocathode, is given by:

$$P_R' = \frac{\rho e^{-2\gamma r} A_R}{2\pi r^2 x 10^{10}} T_o T_F P_o \left(\frac{\Delta t_o}{\Delta t_R}\right) \qquad (1)$$

where ρ = reflectivity of target

γ = 3.9/V (V = visibility in km)

r = range of target (km)

A_R = effective receiver area (cm^2)

T_o = transmission of receiver optical system

T_F = product of transmission of all filters used

P_o = peak power of transmitted laser pulse

Δt_o = width of initial laser pulse

Δt_R = " " received pulse

The derivation of Equation 1, along with the assumptions underlying it, can be found in Sections 3.3 and 4.3 of Reference 1.

Background

The average power P_B from the background, falling on the photocathode, is given by:

$$P_B = \bar{P}_B (\Delta\lambda \cdot \Omega_R \cdot A_R) \quad T_o T_F \qquad (2)$$

Where $\bar{P}_B$ = Spectral radiance of sunlit target ($W/\text{Å}/ ster/cm^2$) The target is assumed to fill f.o.v.

$\Delta\lambda$ = bandpass of optical filter (Å)

Ω_R = solid angle f.o.v. = $\pi\Theta^2/4$, where Θ = full angle f.o.v.

A_R = effective area of receiver (cm^2)

T_o, T_F = transmission as defined for Eq. (1) above.

Signal to noise

The ratio of peak signal current i_S to the rms noise current $\bar{i}_N$ at the photomultiplier output is given (for background-limited systems) by

$$i_S/i_N = \frac{(\eta)^{1/2} P'_R}{(2Bh\nu P_B)^{1/2}} \qquad (3)$$

where η = quantum efficiency of detector

B = electronic bandwidth (Hz)

$h\nu$ = energy of laser photon = 2.4×10^{-19} joules

Equation 3 holds in general only if $P_B > P'_R$; otherwise a sizeable signal will also have fluctuations which could contribute more noise than the background fluctuations. However, in the application envisioned for the fog bank detector, return signals above a fixed threshold will be used to trigger an alarm. In this case the significant S/N ratio is obtained from the magnitude of the signal and the rms noise in the absence of signal. Therefore Equation 3 will be applicable here regardless of the relative sizes of P_B and P'_R.

In addition to the use of the three above relations, some information is obtained directly from the oscillograms. For example, the broadening of the return pulse, or the ratio $(\Delta t_o/\Delta t_R)$, is determined this way.

Over 100 oscillograms of return pulses were recorded under a variety of conditions. Of these, specific data were selected which were representative of these conditions. About 20 oscillograms were examined in detail, showing LIDAR returns from several kinds of formations, including low and medium stratus clouds (e.g., overcast) and cloud banks.

The analysis of the data from the photographs is illustrated with a specific example (see Figure 7). This photo shows

the dual scope trace representing the return from some stratus clouds to the west. The LIDAR was aimed at about 5 to 10° from the horizontal and the scattering occured at the dark underside of the cloud layer.

The values of relevant parameters are found to be:

r = 4.8 Km [obtained from A sweep rate (5 μsec/cm)]

Vis = 15 Km or better

i_s = 400 μA [20 mV anode signal across R_L=50 ohms]

R = 2×10^4 amps/watt [Overall detector responsivity @1000 Vdc]

$P'_R = i_s/R = 2 \times 10^{-8}$ watts [On detector]

i_{Bgd} = 20 μA

$P_B = i_{Bgd}/R = 10^{-9}$ watts [On detector]

$T = T_{ND} \times T_{NB} \times T_{optics} = 3 \times 10^{-3}$ [ND=2; $\Delta\lambda$=100Å; T_{optics}= 0.3]

Ω_R = 80×10^{-6} ster. [Aperture =4.5 mm]

$\bar{P}_B = P_B/(\Omega_R \cdot T \cdot \Delta\lambda A_R) = 3 \times 10^{-7}$ watts/cm^2/Å/Ster

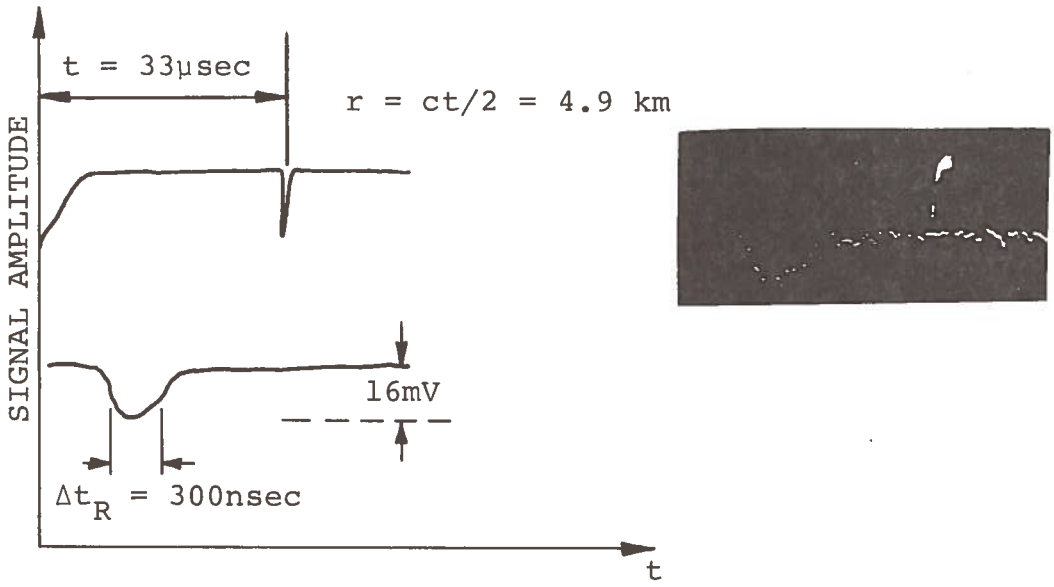

Figure 7. Example of Return Signal from Stratus Clouds (Photo #99-4). A Sweep: 5 μsec/cm; B Sweep: 200 nsec/cm. Vertical Sensitivity: 0.01 V/cm. Scope Camera Has Reduced Dimensions of Photo by a Factor of 2.

In order to examine the internal consistency of the data analysis, it is useful to derive expected values of signal-to-noise and compare with the measurements. Because the calculations of $i_s/\bar{i}_N$ require some quantities as *input* values which must either be assumed or measured, the expected value of $i_s/\bar{i}_N$ will not be entirely independent of the measured ratio. Still, the comparison should show up any gross inconsistency in the data treatment.

The expected value of $i_s/\bar{i}_N$ can be gotten from two somewhat different approaches. In the first, which we will call the semi-empirical approach, the ratio will be calculated from Equation 3 but using measured values of P_R' and P_B. For the sample data analyzed above (#99-4), $(i_s/\bar{i}_N)_{\text{semi-emp.}} = 20$.

A second way to obtain an expectation for the return is to combine Equations 1, 2, and 3, arriving at an *ab initio* expression for $i_s/\bar{i}_N$ in the form:

$$(i_s/\bar{i}_N)_{\text{ab initio}} = \frac{P_o \rho}{2\pi}\left(\frac{\eta A_R}{2h\nu B}\right)^{1/2} \cdot \frac{e^{-7.8r/V}}{r^2} \cdot \left(\frac{\Delta t_o}{\Delta t_R}\right)\left(\frac{T_o T_F}{\bar{P}_B\, \Delta\lambda\, \Omega_R}\right)^{1/2} \tag{4}$$

Taking values for the parameters of #99-4 given above, and using corrected values of ρ and visibility (see below), $(i_s/\bar{i}_N)_{\text{ab init.}} = 11$.

Finally the actually observed ratio $(i_s/\bar{i}_N)_{\text{obs}} = 7$. A comparison of these three values shows reasonable agreement. Table 1 gives similar comparisons for ten different return oscillograms.

The signal P_R', by itself, can also be calculated *ab initio*. Doing so (for the same photo data) gives $(P_R')_{\text{ab init}} = 10^{-8}$ watts. The value observed was 2×10^{-8} watts. This result, along with those in Table 1, is indicative that the analysis of the data has indeed been internally consistent.

TABLE 1. COMPARISON OF RETURN SIGNAL-TO-NOISE RATIOS FOR SEVERAL DIFFERENT BACKSCATTER CONDITIONS. [THE SUFFIXES REFER TO METHOD OF OBTAINING $i_s/\bar{i}_N$, AS DISCUSSED IN TEXT. ONLY NUMBERS IN THE SAME ROW ARE MEANINGFUL IN COMPARISON]

Oscillogram #	$(i_s/\bar{i}_N)_{semiemp.}$	$(i_s/\bar{i}_N)_{ab\ initio}$	$(i_s/\bar{i}_N)_{obs}$	TARGET
58-1	17	5	10	cliff
95-1	25	5	15	"
98-1	1	6	8	cloud
99-4	20	11	7	"
101-2b	10	16	5	"
104-2	34	13	10	stratus
109-1	10	23	8	cloud
110-5	100	78	20	cliff
110-6	15	31	10	cliff
112-1	10	15	5	cloud

Reflectivity

The value of reflectivity ρ can be deduced from Equation 1:

$$\rho = \frac{2\pi P_R' r^2 e^{2\gamma r (10^{10})}}{A_R \cdot T \cdot P_o} \frac{\Delta t_o}{\Delta t_R} = 1.25$$

The above result is clearly suspect, since the maximum possible value for ρ is unity, corresponding to perfect reflectivity. Among the other data analyzed, though the average reflectivity was around 0.6, several values were greater than one.

The major cause of the non-physical results for ρ is thought to be the uncertainty in estimating visibility. Because the visibility was so often inhomogeneous, it is felt that the estimates could be off by as much as 50%. Since the visibility enters the calculations in the exponent, the error in ρ can easily arise.

Pursuing this question further, an overall look at the data indicates that there has been a tendency in general to underestimate V. This may be due to the influence of the haze which often appeared to hang around portions of the bay. The haze tends to reduce the subjective estimate of visibility (by scattering blue light predominantly) whereas the ruby beam is not extinguished by the same amount. If we take the visibility estimates as being 50% too small, then the corrected value of V is $V_C = V(1 + 0.5)$. This leads to a corrected value $\rho_C = (e^{2\gamma r})^{-1/3} \rho$, where $\gamma = 3.9/V$.

For the present example, with $\rho = 1.25$ and $e^{2\gamma r} = 12.2$, we obtain $\rho_C = 0.4\rho = 0.5$. This value is more in line with what one might expect, and indeed, when all the data were treated with the same type of visibility-dependent correction, the average value of ρ_C was approximately 0.3.

Though it appears that this type of systematic correction is sufficient to remove the major error in ρ, there are two other factors that lend some uncertainty. One is the variation of 20% in laser output power. The second is the approximation underlying the appearance of $(\Delta t_o/\Delta t_R)$ in Equation 1. The exact expression, in which the actual pulse widths and shapes are taken into account, could result in a significant (perhaps 50%) change in the value of ρ.

RESULTS AND CONCLUSIONS OF LIDAR TESTS

The analysis of all the LIDAR data leads to the following results:

1. Typical return pulses from bank-like cloud structures and stratus clouds have widths of 150 to 300 nsec, due to broadening by these diffuse targets.
2. The brightest background observed, caused by sun-lit clouds filling the field-of-view of the receiver, was found to produce a spectral radiance at the receiver of 2 μwatts/cm^2/Å/ ster.

3. The effective reflectivity of fog banks was not measured, and the values of ρ_c determined from clouds is not very accurate, as has been noted. However, it seems that choosing a value of $\rho_c = 0.3$ gives consistent results and this value will be used for any future estimates.
4. The variation of the amplitude and shape of return signals from pulse to pulse, within the same cloud target, seemed to be insignificant, indicating that the extent of patches or inhomogeneities in the cloud are comparable to or larger than the scattering length of the cloud. Since the return pulse widths are about 200 to 300 nsec long, this indicates the cloud patches are thicker than $(c \cdot t_R/2)$ or 100 to 150 feet.
5. The atmospheric backscatter has not been discussed yet. The magnitude and duration of this return are important, since they will determine the earliest point in the range scan at which the fog bank can be detected. The typical return from the atmosphere was found to fall, after about 2 μsec, to the peak signal level of a return from a cloud at three miles. Since closer targets will give signals larger by (approximately) the ratio of distances squared, it is felt that detection of banks up to as close as 1/4 mile, and perhaps less, can be accomplished with no interference from the atmospheric return.

The above results are consistent with the assumptions underlying the proposed LIDAR design[1]. Consequently, the system proposed remains valid from a technical point of view. However, these tests were not able to resolve certain questions of an operational nature, as will be pointed out in the Summary and Conclusions.

INFRARED RADIOMETER: FIELD TESTS

A description of the experimental infrared radiometric apparatus appears in Appendix A of Reference 1. The detection was done in a wavelength band 0.2μ wide centered near 9μ. The radiometer had a 2 mrad f.o.v., kept small to permit the angular resolution needed for scans in the neighborhood of the horizon. With a 3 second time constant, the minimum detectable power was found to be 5×10^{-10} watts.

The system used in the Point Bonita tests differs from that described in Reference 1 only with respect to the mechanical telescope scan drive. By gearing down from a synchronous motor speed of 1 rps, a minimum scan speed of 1.62°/min was obtained. The synchronous motor provided more torque that the earlier version, and the improvement in reproducability of the scan was considerable, with no significant slippage. Two microswitches, operating at the upper and lower limits of the vertical scan, allowed the radiometer to be run continuously and automatically. The most commonly used (angular) sweep rates were $1.62°^{-1}$ min and $3.24°$ min^{-1}, and the entire scan durations were ten minutes and five minutes, respectively. The scan encompassed approximately 15°, from below the reference rail (see below) to well above the horizon.

The radiometer was situated inside the generator house, with a southern exposure through an open window, as shown in Figure 2 (position marked B). The scan was made in a vertical plane which ran almost directly north-south.

The elevation of the radiometer was approximately 100 feet above mean sea level and the calibration of angular scan in terms of distance is therefore essentially the same as that appearing in Figure A.7 (Reference 1) where h = 30 m. The procedure for scanning was similar to that previously described with the exception of the reference object used. In the Point Bonita setting, there were no land-based targets to serve as a scan reference index. Instead a piece of the railing along the

walkway served this purpose. As the scan proceeded upwards in angle, the yellow reference rail (always warmer than the water) caused a reference signal to be present on the recorder trace. This allowed distances near the horizon to be referenced to the fixed angular position of the rail.

RESULTS

Although numerous runs were made under varying weather conditions, the results of the radiometer tests can effectively be discussed with reference to a few typical situations. These are shown in Figures 8a thru 8f. The significance of the graphs and the parameter α is identical to that in Chapter 3, Reference 1. Briefly, α is the scan angle of the radiometer.

The traces were taken with the same gain but in some cases a time constant of 0.1 sec was used; in others, about 3 sec. The position of the reference rail, which always appears warmer than the water, is indicated by the vertical line running through the peaks on the left side of the trace. The position of the horizon (as determined by the clear day recording) is indicated by the right hand vertical line. No attempt was made to determine an absolute temperature calibration.

The main features of the data and the conclusions drawn from them, are:

- Figure 8a: On a clear day, the horizon is clearly seen, first as a rise in effective temperature, followed by the appearance of the colder sky. The origin of this bump at the horizon has been discussed on page 21 of Reference 1.
- Figure 8b: As in Figure 8a, this was taken on a clear day, but the horizon appeared hazier. Perhaps there was some smog lying off-shore. There is an indication of a rise in signal slightly before the horizon angle. This type of premature upward turning of the trace (i.e., before the horizon is reached) was seen on several days even though for visibility purposes, no seeing problem existed. Note that the difference in noise between Figure 8a and 8b

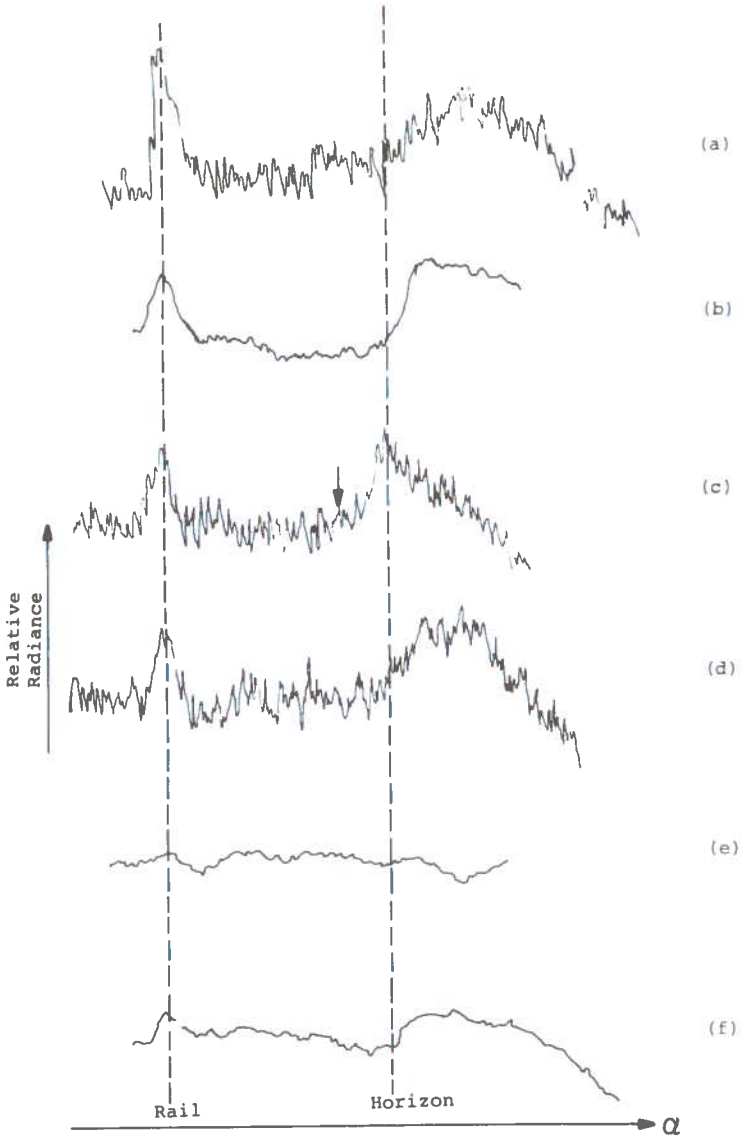

Figure 8. Recorder Traces Showing Radiance as Seen by Vertically-Scanning Infrared Radiometer. Wavelength = 9 microns. Vertical Line on Left-Hand Side Shows Position of Reference Rail. Line on Right-Hand Side Gives Position of Horizon. (a) Clear Day with Horizon Visible Through Haze. Taken at 4:00 PM. (b) Similar to (a) But Somewhat Hazier. (c) Fog Bank, Indicated by the Increase in Slope Before the Horizon is Reached. 6:30 PM. (d) About One Hour After (c). Bank Appears to be Lifting or Thinning. (e) Low Overcast but Good Visibility. 11:30 AM. (f) Night (9:00 PM) with Clear Sky.

is due primarily to the use of a longer time constant in the latter.

· Figure 8c: Here, a pre-horizon upturn is seen (arrow) and is due to the presence of a fog bank. Although the bank appeared to the eye to be at least three or four miles away, the position of the arrow, where the slope begins to change, corresponds roughly to a distance of about one mile. The visibility was such that land features several miles away were clearly visible.

· Figure 8d: This trace was recorded about one hour later than 8c. The bank appears by eye to be receding or lifting and this is indicated by the radiometer also.

· Figure 8e: Taken at 11:30 am on a day when visibility was good but a low overcast had excluded the direct sun all morning. In addition, a rather brisk wind was blowing. The overall effect was a general washing out of the brightness temperature differences characteristic of the previous traces. In an operational system, the reference would not depend on the sun for its source of heat. However, the features near the hozizon are more important. The usual bump at the horizon has vanished, apparently due to the equalization of the brightness temperatures from horizon features. This is a potential source of ambiguity, since under these conditions, fog banks might go undetected.

· Figure 8f: This is a trace recorded at 9:00 pm. Already due to radiative cooling, the solar-induced temperature gradients have begun to disappear. Since a fog bank was not observed at night, we cannot make statements about its detectability under these conditions. The initial formation of fog banks is related to temperature differences between the water surface and a mass of moist air. The evolution of this temperature difference with the development and motion of the bank is not known.

SUMMARY AND CONCLUSIONS WITH REGARD TO POINT BONITA TESTS

SUMMARY OF TESTS

LIDAR:

Width of return pulses: 150-300 nsec.

Average reflectivity: 0.3

Background radiance (max.): 2 μwatts/cm^2/Å/ster.

Atmospheric backscatter will not interfere with bank detection, for banks farther than 1/4 mile.

Assumptions underlying LIDAR prototype design[1] hold up as technically sound.

Infrared Radiometer:

Haze and/or smog banks can be mistaken for fog bank.

Seasonal variations could not be determined, but are probably significant.

No fog banks were observed at night or on overcast days. Indications are that under such conditions, detectability may be hampered due to the tendency for temperature differences to "wash out".

Too many ambiguities to be a practical method, at this time.

Operational Unknowns:

Due to the lack of occurrence of fog banks during the test period at Point Bonita, certain operational questions still remain unanswered. This can be summarized as follows:

Do the fog banks have certain physical properties which might complicate their detection? For example, do they sometimes move well above the sea surface and only descend to the surface when almost on shore?

Do fog banks sometimes slip in just above the water, the entire mass staying so low that a fixed laser beam might be directed above it and so miss it entirely?

Are there many situations where banks can approach from one of several directions (including from behind

the detector), preventing detection until a general condition of prevailing fog has set in?

For the typical installation site, is it necessary to employ horizontal scanning?

CONCLUSIONS: PREDICTIONS FOR GaAlAs LIDAR PERFORMANCE:

The LIDAR design proposed in Reference 1 includes a GaAlAs laser array for the transmitter. Based on the results of the Point Bonita field tests, it is possible to predict its performance with increased confidence and such an analysis is presented below. Unless otherwise indicated, the values used for the parameters are taken from[1].

We will use Equation 4 to predict the S/N ratio for the system. First, a list of parameters which we regard as essentially invariable in our considerations:

P_o = 500 watts [maximum out of transmitter]

λ = 8200Å [Also, $h\nu = 2.4 \times 10^{-19}$ Joules]

Δt_o = 150 nsec

Δt_R = 300 nsec

T = overall attenuation of receiver optics = 0.5

η = 0.04 (e.g., RCA C31025C)

$\Delta\lambda$ = 100Å

B = 3×10^6 cps

The system parameters which we will consider variable are the transmitter beam divergence (and accordingly the receiver f.o.v.), and the diameter (and hence the area A_R) of the receiver optics. Though the amount of variation considered is only a factor of two for each of these quantities, there is a significant improvement in the performance of the system with smallest f.o.v. and largest (practical) receiver area. At the same time, however, there will be an increase in the cost, size and complexity of the system.

In addition, the performance estimate depends on the background intensity. Though the maximum background measured was 2 μwatts/cm^2/ster/Å, one-tenth this value was found for an

overcast (but otherwise clear visibility) day. Even on a sunny day, if the field of the receiver is not filled with a sun-lit cloud, the noise is less than the maximum value. And of course, at night, the background will no longer affect the performance. System performance is also analyzed below with a background of 0.2 μwatts/cm^2/Å/ster.

Finally, the analysis is based on the use of a photomultiplier detector. The potential advantages of an avalanche photodiode detector, particularly in background-limited situations, have been pointed out previously. Though the photodiode appears to give real improvement on paper, our lack of experience with this device, and with the signal processing techniques which would accompany its use, prohibit us from recommending it in the initial system. We feel that the first system built should incorporate the familiar photomultiplier. Once this system's performance and operational limitations are understood, the improvement promised by the solid-state detector can be explored.

Using the above parameters, we estimate the performance of a GaAlAs laser. The performance is given in terms of the range r at which the signal-to-noise (averaged over 100 pulses) is such as to yield 95% detection probability and a (single-pulse) false alarm probability of 2×10^{-7}, as discussed in Reference 1. The atmospheric visibility is taken as 12 km ($\gamma = 0.32\text{km}^{-1}$).

Case 1: $P_B = 2 \times 10^{-6}$ watts/cm^2/ster/Å

$\theta = 2°$; $\Omega_R = 9 \times 10^{-4}$ ster

$A_R = 470$ cm^2 (Diam. = 10") r = 1.75km

Case 2: $P_B = 2 \times 10^{-7}$ watts/cm^2/ster/Å

$\theta = 2°$

$A_R = 470$ cm^2 (D = 10") r = 2.5km

Case 3: $P_B = 2 \times 10^{-6}$ watts/cm^2/ster/Å

$\theta = 1°$; $\Omega_R = 2.2 \times 10^{-4}$ ster

$A_R = 1700$ cm^2 (D = 20") r = 2.6km

Case 4: $P_B = 2 \times 10^{-7}$ watts/cm^2/ster/Å

$\theta = 1°$

$A_R = 1700$ cm^2 (D = 20") r = 3.5km

REFERENCES

1. Lifsitz, J. R., Ingrao, H. C., *Two Candidate Systems for Unmanned Fog Bank Detection*, Report No. DOT-TSC-CG-71-3, Transportation Systems Center, Cambridge, Mass., June, 1971.